Journal of Solid State Chemistry 184 (2011) 2683–2689

Contents lists available at ScienceDirect

Journal of Solid State Chemistry

journal homepage: www.elsevier.com/locate/jssc

The influence of diffusion temperature on the structural, optical and magnetic properties of manganese-doped zinc oxysulfide thin films

İ. Polat [a], S. Aksu [b], M. Altunbaş [a,*], S. Yılmaz [a], E. Bacaksız [a]

[a] Department of Physics, Karadeniz Technical University, 61080 Trabzon, Turkey
[b] SoloPower Inc., 5981 Optical Ct., San Jose, CA 95138, USA

ARTICLE INFO

Article history:
Received 12 April 2011
Received in revised form
6 July 2011
Accepted 11 July 2011
Available online 10 August 2011

Keywords:
Semiconductors
Thin films
Mn-doped zinc oxysulfide
XPS
Annealing
Ferromagnetism

ABSTRACT

We investigated the structural, optical and magnetic properties of Mn-doped zinc oxysulfide films. Zn(O,S) films were deposited by a spray pyrolysis method on glass substrate. A thin Mn layer evaporated on these films served as the source for the diffusion doping. The XRD pattern of undoped films revealed the presence of two wurtzite phases corresponding to ZnS and ZnO with a strong preferred orientation along the ZnS (0 0 2) hexagonal plane direction. SEM showed a similar surface morphology for the undoped and Mn-doped films, displaying regular arrays of hexagonal micro-rods perpendicular to the substrate. The optical transmission measurements showed that both undoped and Mn diffusion-doped films had a low average transmittance less than about 10%. The gap energy is decreased from 3.42 to 3.33 eV upon annealing at 400 °C. Photoluminescence studies at 300 K show that the incorporation of manganese leads to a decrease of deep level band intensity compared to undoped sample. Clear ferromagnetic loops were observed for the Mn-doped Zn(O,S) films, which might be due to the presence of point defects.

1. Introduction

In the last few decades, there has been a great deal of interest in the study of diluted magnetic semiconductors (DMSs), in which a fraction of non-magnetic host cations are replaced by transition metal (TM) atoms such as Mn, Cr, Fe, Co and Ni. DMSs are promising materials for spintronics devices due to the capability of utilizing both the charge and spin degree of freedom. The use of spin appears promising for a large group of devices such as non-volatile memories, ultra-fast optical switches, spin valve, spin light emitting diodes and spin field effect transistors [1–9]. High Curie temperatures are essential for practical applications of DMSs in spintronic devices. Initially, the research effort was concentrated on two major DMSs, namely (Ga,Mn)As [10] and (In,Mn)As [11]. Calculations based on the Zener mean-field model of ferromagnetism by Dietl et al. [12] predicted a room-temperature ferromagnetism in ZnO-based DMSs and initiated an intensive research effort on the investigation of magnetic properties of TM-doped semiconductors [13,14]. II–VI compound semiconductors doped with magnetic ions have been obtained by several researchers with various properties such as ferromagnetism [14], spin-glass behavior [15] and paramagnetism [16]. These magnetic properties were found to be strongly dependent on the synthesis method, the concentration of TM atoms and the sample preparation conditions.

ZnO is one of the most favorable oxide semiconductors for potential applications in the optoelectronics field due to its wide band gap (3.37 eV) and large exciton binding energy (60 meV) [17]. Doping with 3*d* TM elements such as Mn, Co, Er and Cu has been found to be promising for potential ZnO-based DMS applications [12,18–20]. Similar to ZnO, zinc sulfide (ZnS) also has a wide bandgap energy of 3.7 eV (bulk) and a large exciton binding energy of 40 meV. ZnS is also a well-known luminescent material, which finds wide applications in the fields of flat-panel displays, lasers and sensors [21–23]. By combining these attractive optical properties with the room temperature ferromagnetism, ZnS might also be a desirable host semiconductor for DMS applications, opening possibilities for the fabrication of a variety of magneto-optic devices. For example, Sarkar et al. [24] reported that the Mn-doped ZnS nanocrystals prepared by a solvothermal technique exhibited ferromagnetic behavior below 30 K. Peng et al. [25] demonstrated that Mn-doped ZnS nanoparticles grown by a co-precipitation reaction exhibited paramagnetic behavior and no antiferromagnetic interaction between Mn^{2+} ions existed. Yuan et al. [16] measured the magnetic properties of Mn-doped ZnS nanowires and observed a paramagnetic behavior at 5 K.

Zinc oxysulfide, Zn(O,S), is a solid solution of ZnO and ZnS. The Zn(O,S) thin films prepared at different mixture ratios of these

* Corresponding author: Fax: +90 462 325 31 95.
E-mail address: altunbas@ktu.edu.tr (M. Altunbaş).

0022-4596/$ - see front matter © 2011 Elsevier Inc. All rights reserved.
doi:10.1016/j.jssc.2011.07.017

two phases might offer unique abilities to tune the electronic and optical properties, which might lead the way to various new applications. ZnS exhibits polymorphism of cubic sphalerite and hexagonal wurtzite phases. Partial substitution of S ions in ZnS with O ions might lead to significant changes in the electrical and optical properties due to the large electronegativity and size difference between the two ions. In addition, bandgap engineering of Zn(O,S) films might be possible due to the different bandgaps of ZnO and ZnS [26,27]. In the area of thin film heterojunction solar cells, particularly copper indium gallium diselenide absorbers, transparent Zn(O,S) films were found to be suitable replacements for toxic CdS films as window layers [28,29]. Although various TM-doped ZnS and ZnO semiconductor systems have been investigated intensively in recent years, there is no much work done on the use of zinc oxysulfide, Zn(O,S), thin films for spintronics applications. Various deposition techniques, such as rf sputtering [30,31], atomic layer deposition [26] and pulsed laser deposition [27] have been reported for the deposition of Zn(O,S), thin films. In addition, Vlasenko and colleagues investigated the effect of oxygen doping on the electro optical, luminescent and photoelectrical characteristics of Mn-doped Zn(O,S) films [32]. In this paper, we have studied the structural, optical and magnetic properties of Mn-doped zinc oxysulfide, Mn-Zn(O,S), thin films, which were grown by spray pyrolysis on glass substrates and diffusion-doped at varying annealing temperatures under vacuum.

2. Experimental

Zinc oxysulfide thin films were obtained by the spray pyrolysis technique in air. The initial solution is prepared from zinc chloride ($ZnCl_2 \cdot 6H_2O$) at 0.05 M and thiourea [$SC(NH_2)_2$] at 0.1 M in deionized water. The prepared solution was sprayed with a glass nozzle onto the glass substrate with a spray rate of about 2 ml/min and a growth rate of $\approx$20 nm/min using air as a carrier gas [33]. The nozzle-to-substrate distance was approximately 20 cm, and spraying time was 210 min. During the growth, the substrates were rotated with a speed of 10 rev/min at a temperature of 490 °C. Zn(O,S) films obtained in this manner had thicknesses ranging from approximately 2.5 to 3.5 μm and exhibited good adherence to the substrate surfaces. Elemental Mn was deposited onto Zn(O,S) thin films using electron beam evaporation. The thickness of the Mn layer was measured by PHE 102 Spectroscopic Ellipsometry and found to be about 400 nm. After Mn deposition, in order to diffuse Mn into the Zn(O,S) structure, the thin films were annealed at temperatures of 300, 350 and 400 °C for 45 min in vacuum of 2×10^{-5} Torr.

The crystal structure was analyzed by X-ray diffraction (Rigaku D/Max-IIIC diffractometer) using Cu$K\alpha$ radiation over the range $2\theta = 20$–60° at room temperature. The surface morphology was studied by means of Zeiss Evo LS10 scanning electron microscopy (SEM). An energy dispersive X-ray spectroscopy (EDS) system in the same tool was used for determining the chemical composition of samples at an applied voltage of 20 kV. Optical transmission data in the 190–1100 nm range was measured with a Shimadzu UV-1601 spectrophotometer. Photoluminescence (PL) measurements were performed at 300 K using SpectraMax M5 and PL spectra were excited with the Xenon Flash Lamp of 1 J/flash. The magnetic properties of films were investigated using Quantum Design PPMS system with the module of vibrating sample magnetometer. The chemical compositions and present bonding types on the surface and near-surface region of the films were examined by X-ray photoelectron spectroscopy (XPS) realized by a Thermo Monochromated high-performance XPS spectrometer system equipped with a Al $K\alpha$ X-ray radiation source of 1486.6 eV energy. The surface of the films was sputtered by Ar ions in order to clean the surface from undesired impurity atoms of C and O atoms.

3. Results and discussion

The structural properties of films were determined using XRD measurements. Fig. 1(a) shows a typical XRD pattern of the undoped Zn(O,S) film grown by spray pyrolysis at 490 °C on a glass substrate. The diffraction pattern of this film revealed a polycrystalline wurtzite crystal structure and the presence of two phases corresponding to ZnS (JCPDS no. 36-1450) [34] and ZnO (JCPDS no. 36-1451) [35] with a strong preferred orientation along the hexagonal (0 0 2) ZnS plane direction. Other characteristic planes for hexagonal ZnS were observed as weak peaks at

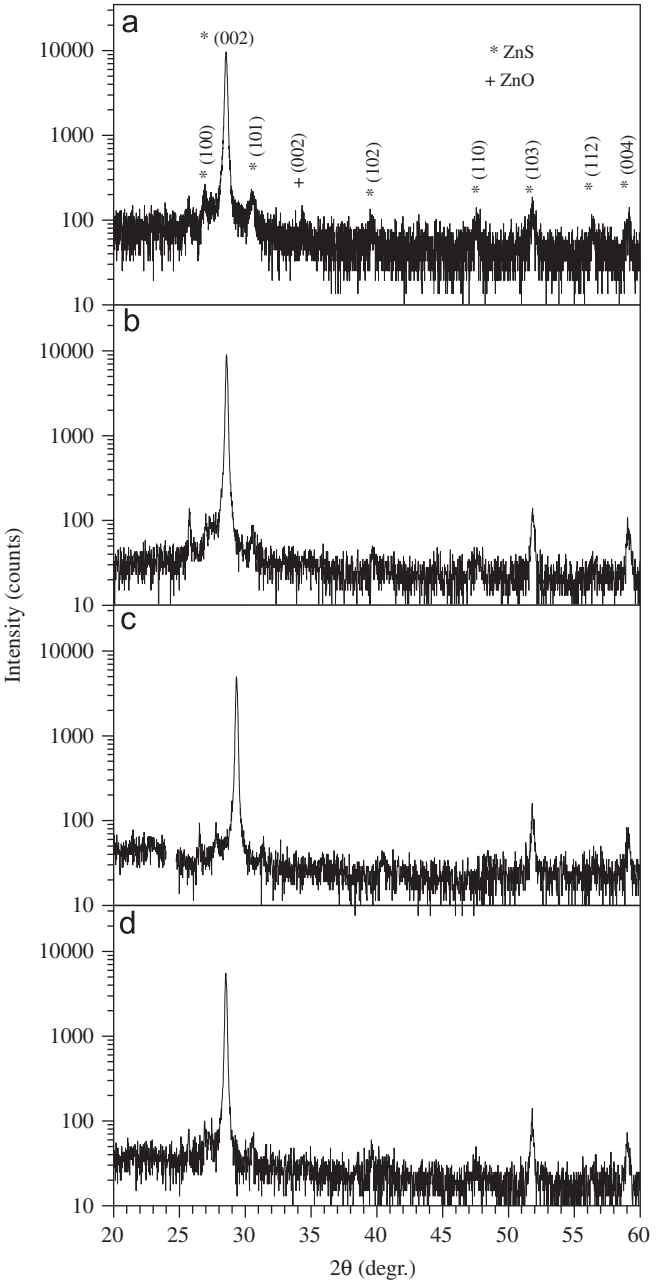

Fig. 1. XRD diffraction patterns of the undoped Zn(O,S) (a), and Mn diffusion-doped Zn(O,S) thin films annealed at 300 °C (b), 350 °C (c) and 400 °C (d).

(1 0 0), (1 0 1), (1 1 0), (1 0 3), (1 1 2) and (0 0 4). In addition, we detected the presence of a small ZnO (0 0 2) peak at $2\theta=34.59^{\circ}$ for both undoped and Mn diffusion-doped Zn(O,S) films.

The XRD patterns of Mn diffusion-doped Zn(O,S) films at 300, 350 and 400 °C in vacuum are also shown in Fig. 1(b)–(d), respectively. It should be noted that our films conserved their hexagonal structure throughout these doping steps. However, the intensity of (0 0 2) peak decreased with the increase in the Mn doping temperature in Zn(O,S) thin films. No other secondary phases related to Mn metal clusters or Mn compounds such as MnO, MnO_2, MnS, etc. were detected in these samples, at least within the limit of X-ray detection. The lattice parameter of samples, *c*, was calculated from the position of high intensity of the ZnS (0 0 2) peak, yielding to be 0.6243 nm for the undoped and 0.6255 nm for Mn-doped Zn(O,S) thin films at 400 °C. One possible reason for the increase in the lattice parameter with doping might be the replacement of Zn ions by Mn ions as the ionic radius of Mn^{2+} (0.80 Å) is larger than the ionic radius of Zn^{2+} (0.74 Å) in tetrahedral coordination [36]. It is known that the variation in the lattice parameter *c* depends on several parameters such as uniform stress, incorporation of impurities with different ionic radius into the lattice, shift in stoichiometry, etc. For this reason, the change in the *c* parameter observed in the present work occurs as a combined effect in view of the competing effects either increasing or decreasing trends in the value of *c*. For example it is reported that lattice constant decreases as Cd concentration increases in CdTe thin film [37].

Chemical compositions of undoped Zn(O,S) and Mn diffusion-doped Zn(O,S) films at 300, 350 and 400 °C were investigated by EDS at 20 kV and listed in Table 1. As can be seen from this table Mn was detected in all the doped samples and its concentration increased with higher annealing temperatures. Table 1 also shows that the atomic ratio of Zn/O for undoped Zn(O,S) and Mn diffusion-doped Zn(O,S) samples were almost 1. However, compared to undoped ZnO, Mn diffusion-doped Zn(O,S) samples showed slightly lower sulphur content, indicating evaporation of the sulphur atoms of the film surface during the annealing process [38].

SEM surface micrographs shown in Fig. 2 reveal that the surface morphology was similar for the undoped and Mn-doped Zn(O,S) thin films prepared at various annealing temperatures, displaying hexagonal shaped micro-rods. Consistent with the XRD pattern in Fig. 1, the hexagonal rods were found to be regular and almost perpendicular to the substrate, indicating that rods preferentially grow along the (0 0 2) ZnS plane.

Fig. 3 shows an XPS survey spectrum of the Mn diffusion-doped Zn(O,S) thin films annealed at 350 °C. The chemical nature

Table 1
Atomic concentrations of Zn, O, S or Mn determined by EDS at 20 kV in undoped and Mn diffusion-doped Zn(O,S) thin films.

Sample	Measured at%			
	Mn	Zn	O	S
Undoped Zn(O,S)	–	30.8	31.0	38.2
Mn diffusion-doped Zn(O,S) annealed at 300 °C	3.9	35.7	34.1	26.3
Mn diffusion-doped Zn(O,S) annealed at 350 °C	7.1	29.5	30.9	32.5
Mn diffusion-doped Zn(O,S) annealed at 400 °C	8.3	29.3	27.7	34.8

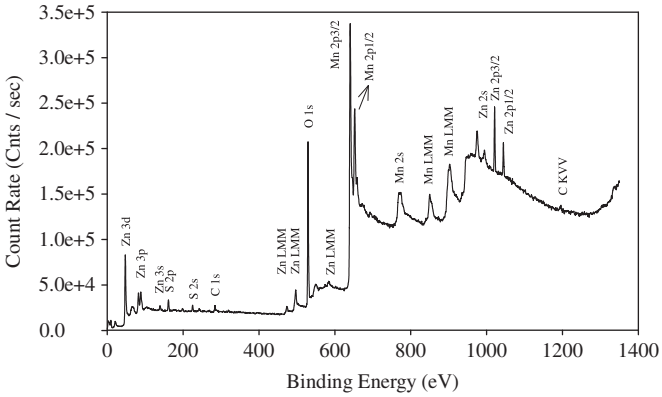

Fig. 3. X-ray photoelectron spectrum (XPS) of the Mn-doped Zn(O.S).

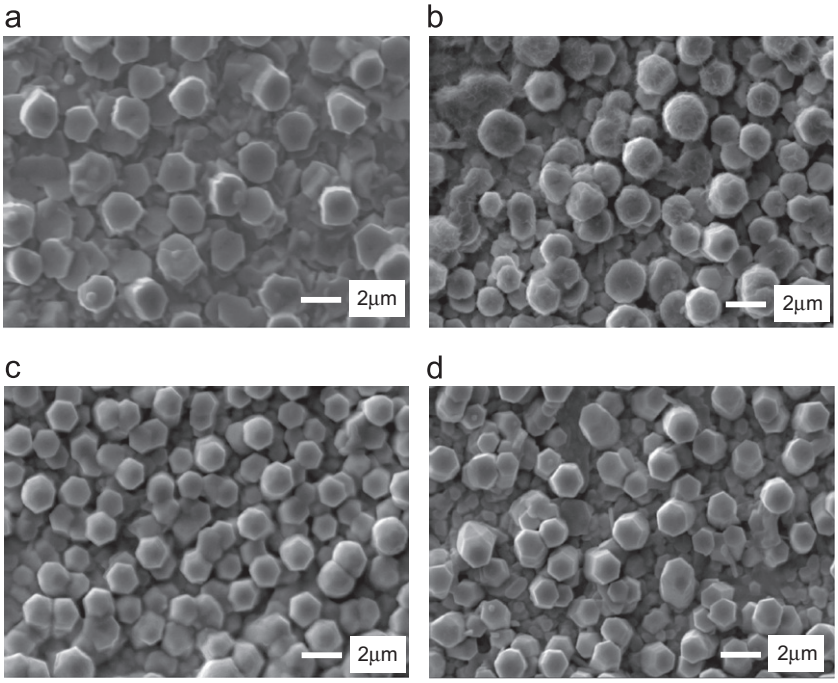

Fig. 2. SEM images of the undoped Zn(O,S) (a), and Mn diffusion-doped Zn(O,S) thin films annealed at 300 °C (b), 350 °C (c) and 400 °C (d).

of the surface of Mn diffused Zn(O,S) thin films were investigated in detail by XPS measurement. Fig. 3 indicates the XPS survey spectrum for the films after the surface was sputtered to reduce the concentration of undesired impurity atoms of C and O down to acceptable values. Comparing with the experimentally proved binding energy values, the survey spectrum indicates the presence of Zn, Mn, S, C and O elements on the surface and near surface region of the films as assigned in Fig. 3. As can be seen from Fig. 4, the Mn 2*p* level splits into a doublet with an energy separation due to spin–orbital angular momentum interaction [39]. Following the peak fitting analysis (Fig. 4), it can be seen that Mn 2*p*3/2 photoelectron peak is decomposed into three peaks whose binding energy values are 640.0, 641.1 and 642.8 eV corresponding to MnO [40], MnS [39] and MnO_2 or Mn_2O_3 [41,42], respectively. From this information, it can be deduced that Mn atoms were chemically bounded to both O and S atoms. In addition to these peaks, a satellite peak at a binding energy of 646.7 eV and a peak due to Mn 2*p*1/2 at 653.2 eV were also recorded. However, no sign of metallic Mn clusters (637.7 eV for Mn 2*p*3/2) was found.

A plot of optical transmittance spectra of the undoped and Mn diffusion-doped Zn(O,S) films as a function of wavelength is shown in Fig. 5. The optical transmission measurements showed that both undoped and Mn diffusion-doped films had a low average transmittance less than about 10%. As can be seen in Fig. 5, the optical band edge shifts to the higher wavelengths with the increasing annealing temperature. After the Mn diffusion-doped Zn(O,S) sample annealed at 300 °C, the transmittance is decreased significantly compared with the one for the undoped Zn(O,S) thin film. This behavior is expected due to the excess Mn on the film surface. As the annealing temperature is increased, the transmittance is improved due to the expected diffusion of Mn ions into the Zn(O,S) films.

The optical band gap energy E_g was calculated from the absorption spectra using the dependence of the absorption coefficient (α) on the photon energy

$$\alpha(h\nu) = A(h\nu - E_g)^{1/2}$$

where E_g is the optical band gap of thin films and A is constant. Fig. 6 shows the plots of $(\alpha h\nu)^2$ vs. $(h\nu)$ for the undoped and Mn diffusion-doped Zn(O,S) thin films. Extrapolation of the linear portions of the plots onto the energy axis gave the band gap values of the films. The gap energy is decreased from 3.42 to 3.33 eV upon annealing at 400 °C. The decreasing of band gap with increasing the annealing temperature might be mainly due to the *sp–d* exchange interactions between the band electrons and the localized *d* electrons of the Mn ions substituting host ions [36,43].

The effect of Mn diffusion-doping on optical emission and defect formation was investigated by PL measurements. Room temperature PL emission spectra of undoped and Mn diffusion-doped Zn(O,S) films annealed at 300 °C, 350 °C and 400 °C are shown in Fig. 7 (a)–(d), respectively. As can be seen from Fig. 7, all the samples exhibited a broad emission band displaying a maximum at about 460 nm. This broad emission band might be due to the presence of intrinsic defects such as oxygen vacancy (V_o), zinc vacancy (V_{Zn}), interstitial zinc (Zn_i), sulfur vacancy (V_S) and interstitial sulfur (S_i) [44–46]. Several other studies on doped ZnS and ZnO films also revealed that the PL response was highly associated with the existing point defects in the film. For examples, Kripal and co-workers observed that PL spectra of their ZnS:Mn^{2+} nanoparticles displayed some emission peaks located at 417, 446, 480 and 520 nm which was attributed to S_i, Zn_i, V_S and V_{Zn}, respectively [47]. Another study on ZnS:Mn^{2+} nanoparticles postulated that the peak at 445 nm was related to recombination of electrons at sulfur vacancy donor level with holes trapped at the zinc vacancy acceptor level [48]. Liu and collaborators showed that Cr doped ZnO samples had some point defects centered at 405 nm, 438 nm and 490 nm that correspond

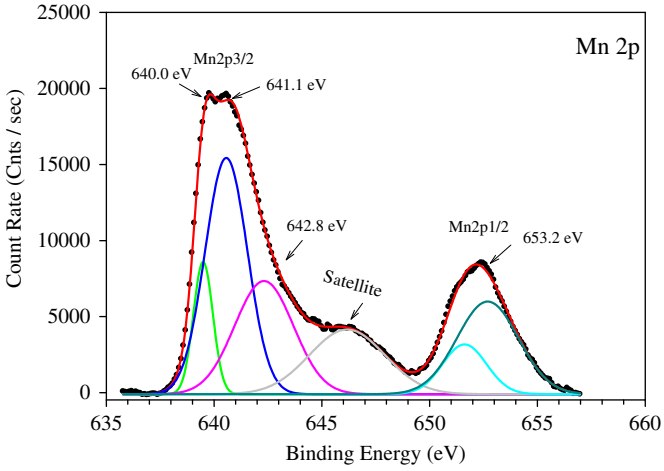

Fig. 4. X-ray photoelectron spectrum (XPS) of the Mn diffusion-doped Zn(O,S) sample at 350 °C for the Mn 2*p* core.

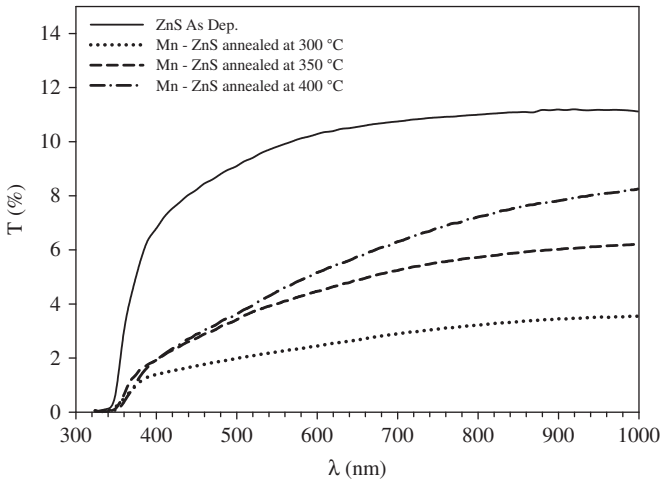

Fig. 5. The optical transmission spectra for undoped Zn(O,S) thin film, and Mn diffusion-doped Zn(O,S) thin films.

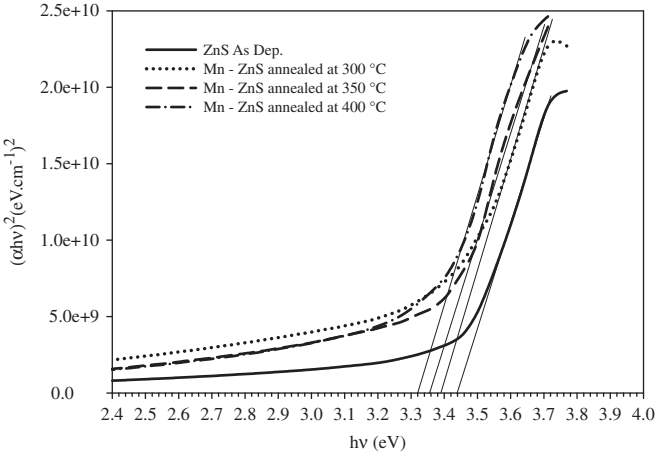

Fig. 6. The plot of $(\alpha h\nu)^2$ vs. photon energy of undoped Zn(O,S) thin films, and Mn diffusion-doped Zn(O,S) thin films prepared by annealing prepared by annealing at 300 °C, 350 °C and 400 °C at 300 °C, 350 °C and 400 °C.

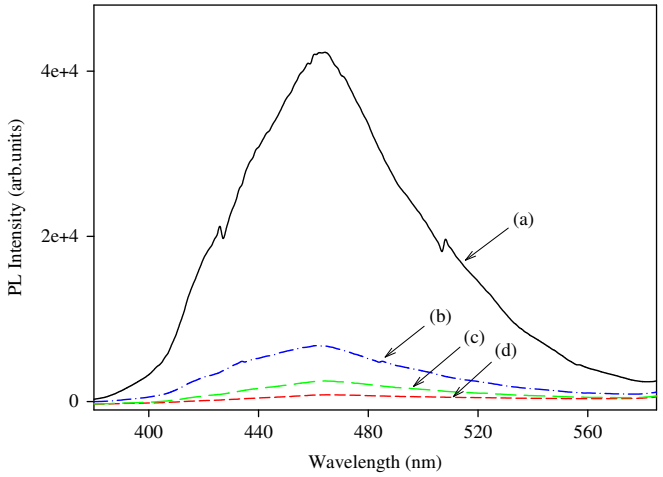

Fig. 7. Room temperature PL spectra of undoped and of Mn diffusion-doped Zn(O,S) thin films prepared by annealing at 300 °C, 350 °C and 400 °C.

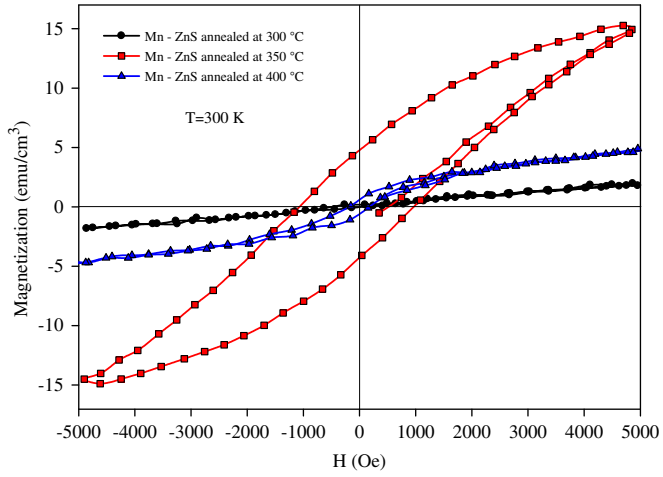

Fig. 8. *M–H* variation of Mn diffusion-doped Zn(O,S) thin films measured at 300 K.

to V_{Zn}, Zn_i and V_o, respectively [49]. The decrease in the PL intensity with doping in Fig. 7 might suggest that the undoped Zn(O,S) film had the highest level of point defects and Mn diffusion-doping leads to lower defect concentrations due to a decrease of the numbers of self-activated centers related with the lattice defects of the zinc sulphide [50].

Field dependent magnetization (*M–H*) curves of Mn diffusion-doped films annealed at 300 °C, 350 °C and 400 °C and measured at 300 K are shown in Fig. 8. As seen from Fig. 8, the Mn diffusion-doped Zn(O,S) films prepared at 350 °C and 400 °C show a clear hysteresis loop as a function of magnetic field, implying ferromagnetic behavior with the coercive field values 1051 Oe, 152 Oe and with the remanent magnetizations 4.86 emu/cm^3, 0.7 emu/cm^3, respectively. As shown in *M–H* loops, the saturation magnetization, M_s, of the sample annealed at 300 °C was found to be lower than that of the other two samples annealed at 350 and 400 °C, displaying a mixed ferromagnetic and paramagnetic behavior, but dominantly paramagnetic one. This behavior was attributed to the formation of a Mn layer on the film surface which itself exhibits a paramagnetic behavior. As the annealing temperature increases to 350 °C, excess Mn atoms diffuse into the Zn(O,S) thin film causing the increase in ferromagnetic properties of the sample. However, it was observed that M_s value decreased as the annealing temperature reached to 400 °C, indicating a deterioration in the ferromagnetism for Mn diffusion-doped Zn(O,S) sample annealed at 400 °C. As illustrated in Table 1, the Mn concentration increased continuously with the increase of annealing temperature for the Mn diffused Zn(O,S) samples. Several previous studies suggest that occurrence of antiferromagnetic coupling might increase due to the shorter separation distances between Mn pairs with increasing Mn concentration, which might lead to a suppressing of the ferromagnetic interaction [51–53]. Accordingly, the deterioration at 400 °C can be explained by the ferromagnetic–antiferromagnetic competition arising from higher Mn concentrations at this annealing temperature.

Several experimental groups have reported that the intrinsic defects played a crucial role in the ferromagnetism of TM-doped ZnO and ZnS films. For example, Yan et al. pointed out that oxygen vacancies played an important role in the appearance of room temperature ferromagnetism for Mn-doped ZnO nanorods [54]. Liu et al. indicated that point defects such as Zn_i or V_{Zn} were responsible for ferromagnetism in Cr:ZnO samples [48]. On the other hand, Bi et al. showed that Co-doped ZnS nanocrystal samples exhibited ferromagnetic behavior in the room temperature, which was explained in terms of point defects such as sulfur vacancies [55].

The possible origins of the ferromagnetism observed in our films might be assessed by considering the results from XRD, XPS and optical measurements. The first possibility is the formation of the secondary phases such as MnS, MnO, MnO_2 and Mn_2O_3. However, these impurity phases MnS, MnO, MnO_2 and Mn_2O_3 are well known to be antiferromagnetic below their Neel temperatures of 152, 116, 92 and 76 K, respectively [56,57]. Hence, the ferromagnetic behavior of the Mn diffusion-doped Zn(O,S) films might not be explained in terms of the formation of the secondary phases. It is also well known that Mn is a paramagnetic material, and cannot contribute to ferromagnetic behavior itself. XPS results clearly showed that there were no Mn clusters in the samples. The observed ferromagnetic behavior might be explained by the coexistence of antiferromagnetic interactions between the second neighbors Mn spins through indirect Mn–S–Mn exchange [58,59]. In addition to this, we also consider that the observed ferromagnetism at room temperature is an intrinsic property of Mn diffusion-doped Zn(O,S) films. As discussed previously, PL spectra can provide information on optically active deep level defects in the Mn diffusion-doped Zn(O,S) films. According to PL results, Mn diffusion-doped Zn(O,S) samples show evidence of a considerable population of point defects such as oxygen vacancies, zinc vacancies, zinc interstitials and sulfur vacancies that may play significant roles, consistent with the

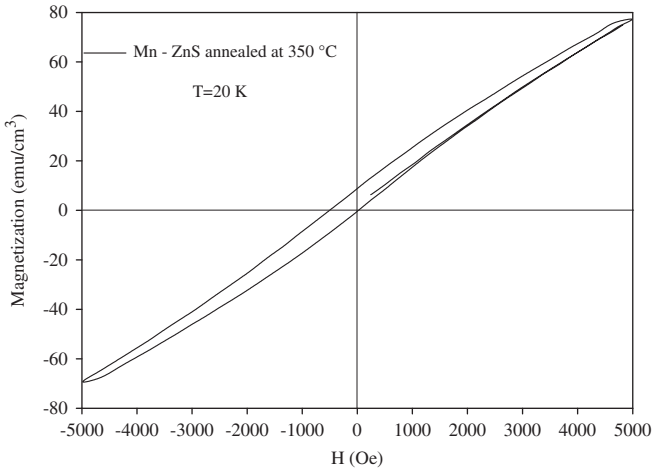

Fig. 9. *M–H* variation of Mn diffusion-doped Zn(O,S) thin films measured at 20 K.

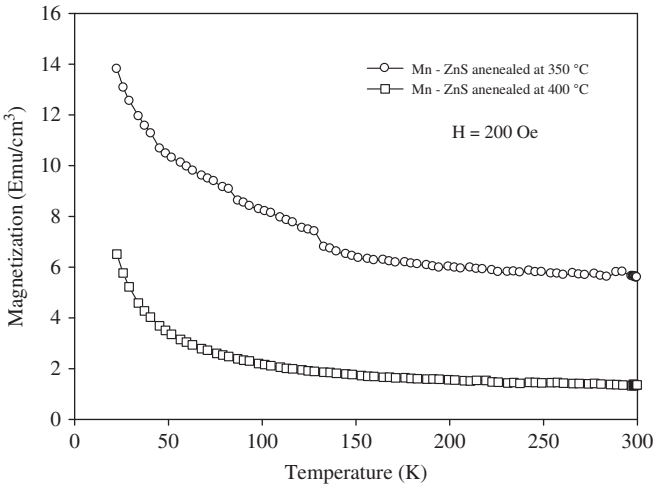

Fig. 10. Temperature dependence of magnetization of Mn diffusion-doped Zn(O,S) thin films.

hypothesis that such defects may be the origin of room temperature ferromagnetism observed in our samples [55,60].

Fig. 9 shows the magnetization as a function of magnetic field measured at 20 K for the Mn–Zn(O,S) sample prepared at 350 °C. From the *M–H* curve, the coercive field and remanent magnetization values were determined to be higher than those measured at room temperature. Similar results were obtained by Kim et al. for (Mn,Zn) co-doped CdS nanowires [61]. This sample exhibits a large magnetic hysteresis loop, indicating its ferromagnetism; however, the center of the loop has shifted about 502 Oe in the negative direction of the magnetic field axis. It was reported that the shift of the magnetic hysteresis loop along the magnetic axis might be explained by exchange-biased coupling at the interface of the ferromagnetic/antiferromagnetic materials [62,63].

The *M–T* curves were also measured at temperature range of 300 − 20 K for Mn diffusion-doped Zn(O,S) films, shown in Fig. 10. As seen from the graph, the magnetization is almost constant in the temperature range of 300 − 50 K followed by an abrupt increase upon further cooling towards 20 K. The Curie temperature is expected to be well above room temperature, but it is hard to determine the exact value as it exceeds the range of our measurements.

4. Conclusions

The structural, optical and magnetic properties of the Mn-doped zinc oxysulfide thin films were investigated. A spray pyrolysis method was used for the deposition of undoped zinc oxysulfide films on glass substrates. Mn diffusion-doping was achieved by annealing zinc oxysulfide films covered with a thin source layer of evaporated Mn, at temperatures ranging from 300C to 400 °C in steps of 50 °C for 45 min under vacuum. XRD results indicated that undoped films exhibited a polycrystalline wurtzite structure and were composed of two phases corresponding to wurtzite ZnS and ZnO with a highly pronounced texture along (0 0 2) ZnS. Surface morphology obtained from SEM was similar for the undoped and Mn-doped films, showing hexagonal micro-rods, which grew perpendicularly to the substrate. EDS analysis revealed a slightly sulfur-deficient chemical composition for all the Mn–Zn(O,S) films as compared to undoped Zn(O,S) sample. Results from XRD and XPS measurements suggested that Mn ions were substituted in place of Zn ions in this film. Both undoped and Mn diffusion-doped films exhibited a low average transmittance. Mn-doping reduced the band gap of the Zn(O,S) films. Band gap decreased with increasing annealing temperatures used in diffusion-doping. Compared to the undoped Zn(O,S) sample, the number of optically active deep level defects decreased for Mn–Zn(O,S) samples. The magnetization measurements as a function of magnetic field and temperature clearly showed room temperature ferromagnetism for the Mn–Zn(O,S) films prepared at 350 and 400 °C and the origin of the observed room temperature ferromagnetism is most likely due to the intrinsic defects.

References

[1] J.K. Furdyna, J. Appl. Phys. 64 (1988) R29–R64.
[2] S.V. Molnar, D. Read, Proc. IEEE 91 (2003) 715–726.
[3] H. Ohno, Science 28 (1998) 951–956.
[4] S.J. Pearton, W.H. Heo, M. Ivill, D.P. Norton, T. Steiner, Semicond. Sci. Technol. 19 (2004) R59–R74.
[5] S.J. Pearton, C.R. Abernathy, M.E. Overberg, G.T. Thaler, D.P. Norton, N. Theodoropoulou, A.F. Hebard, Y.D. Park, F. Ren, J. Kim, L.A. Boatner, J. Appl. Phys. 93 (2003) 1–13.
[6] S.A. Wolf, D.D. Awschalom, R.A. Buhrman, J.M. Daughton, S. von Molnár, M.L. Roukes, A.Y. Chtchelkanova, D.M. Treger, Science 294 (2001) 1488–1495.
[7] J.M. Kikkawa, D.D. Awschalom, Nature 397 (1999) 139–141.
[8] T. Dietl, Semicond. Sci. Technol. 17 (2002) 377–392.
[9] Y.Z. Yoo, T. Fukumura, Z. Jin, K. Hasegawa, M. Kawasaki, P. Ahmet, T. Chikyow, H. Kainuma, J. Appl. Phys. 90 (2001) 4246–4250.
[10] S. Koshihara, A. Oiwa, M. Hirasawa, S. Katsumoto, Y. Iye, C. Uramo, H. Takagi, H. Munekata, Phys. Rev. Lett. 78 (1997) 4617–4620.
[11] A.M. Nazmul, S. Sugahara, M. Tanaka, Phys. Rev. B 67 (2003) 241308–241311.
[12] D. Dietl, H. Ohno, F. Matsukura, J. Cibert, F. Ferrand, Science 287 (2000) 1019–1022.
[13] S.J. Potashnik, K.C. Ku, S.H. Chun, J.J. Berry, N. Samarth, P. Schiffer, Appl. Phys. Lett. 79 (2001) 1495–1497.
[14] Ü. Alver, E. Bacaksız, E. Yanmaz, J. Alloys Compd. 456 (2008) 6–9.
[15] T. Fukumura, Z. Jin, M. Kawasaki, T. Shono, T. Hasegawa, S. Koshihara, H. Koinuma, Appl. Phys. Lett. 78 (2001) 958–960.
[16] H.J. Yuan, X.Q. Yan, Z.X. Zhang, D.F. Liu, Z.P. Zhou, L. Cao, J.X. Wang, Y. Gao, L. Song, L.F. Liu, X.W. Zhao, X.Y. Dou, W.Y. Zhou, S.S. Xie, J. Cryst. Growth 271 (2004) 403–408.
[17] H. Deng, J.J. Russell, R.N. Lamb, B. Jiang, Thin Solid Films 458 (2004) 43–46.
[18] A.J.C. Fiddes, K. Durose, A.W. Bringman, J. Woods, P.D. Coates, A.J. Banister, J. Cryst. Growth 159 (1996) 210–213.
[19] J. Qi, D.Q. Gao, J.H. Liu, W.G. Yang, Q. Wang, J.Y. Zhou, Y.H. Yang, J.L. Liu, Appl. Phys. A-Mater. 100 (2010) 79–82.
[20] Y.F. Tian, Y.F. Li, M. He, I.A. Putra, H.Y. Peng, B. Yao, S.A. Cheong, T. Wu, Appl. Phys. Lett. 98 (2011) 162503–162506.
[21] C. Falcony, M. Garcia, A. Ortiz, J.C. Alonso, J. Appl. Phys. 72 (1992) 1525.
[22] I.T. Sorokina, E. Sorokin, S. Mirov, V. Fedorov, V. Badikov, V. Panyutin, A. Di Lieto, M. Tonelli, Appl. Phys. B 74 (2002) 607–611.
[23] B.X. Fang, Y. Bando, M. Liao, U.K. Gautam, C. Zhi, B. Dierre, B. Liu, T. Zhai, T. Sekiguchi, Y. Koide, D. Golberg, Adv. Mater. 21 (2009) 2034–2039.
[24] I. Sarkar, M.K. Sanyal, S. Kar, S. Biswas, S. Banerjee, S. Chaudhuri, S. Takeyama, H. Mino, F. Komori, Phys. Rev. B 75 (2007) 224409-5.
[25] W.Q. Peng, S.C. Qu, G.W. Cong, X.Q. Zhang, Z.G. Wang, J. Cryst. Growth 282 (2005) 179–185.
[26] B.W. Sanders, A. Kitai, Chem. Mater. 4 (1992) 1005–1011.
[27] S.H. Duelkar, J.-L. Huang, M. Neumann-Spallart, J. Electron. Mater. 39 (2010) 589–594.
[28] E.B. Yousfi, T. Asikainen, V. Pietu, P. Cowache, M. Powalla, D. Lincot, Thin Solid Films 361 (2000) 183–186.
[29] C. Platzer-Björkman, T. Törndahl, D. Abou-Ras, J. Malmström, J. Kessler, L. Stolt, J. Appl. Phys. 100 (2006) 044506–044515.
[30] T. Orent, J. Vac. Sci. Technol. A 9 (1991) 2447–2452.
[31] B.K. Meyer, A. Polity, B. Farangis, Y. He, D. Hasselkamp, T. Krämer, C. Wang, U. Haboeck, A. Hoffmann, Phys. Status Solidi (c) 1 (2004) 694–697.
[32] N.A. Vlasenko, M.B. Kotlyarevsky, Z.L. Denisova, V.V. Kidalov, Y.F. Kononets, A.S. Revenko, L.I. Veligura, Phys. Status Solidi (a) 193 (2002) 338–346.
[33] E. Bacaksiz, M. Tomakin, M. Altunbaş, M. Parlak, T. Çolakoğlu, Phys. B: Condens. Matter 403 (2008) 3740–3745.
[34] H. McMurdie, M. Morris, E. Evans, B. Paretzkin, W. Wong-Ng, L. Ettlinger, C. Hubbard, Powder Diffr. 1 (1986) 77.
[35] H. McMurdie, M. Morris, E. Evans, B. Paretzkin, W. Wong-Ng, L. Ettlinger, C. Hubbard, Powder Diffr. 1 (1986) 76.
[36] P. Singh, A. Kaushal, D. Kaur, J. Alloys Compd. 471 (2009) 11–15.
[37] O. Zelaya-Angel, A. Picos-Vega, R. Ramirez-Bon, F.J. Espinoza-Beltran, Vacuum 41 (1999) 99–102.
[38] H. Metin, F. Sat, S. Erat, M. Arı, J. Optoelectron. Adv. Mater. 10 (2008) 2622–2930.
[39] P.A.G. Beermann, B.R. McGarvey, B.O. Skadtchenko, S. Muralidharan, R.C.W. Sung, J. Nanopart. Res. 8 (2006) 235–241.

[40] R.K. Singhal, M.S. Dhawan, S.K. Gaur, S.N. Dolia, S. Kumar, T. Shripathi, U.P. Deshpande, Y.T. Xing, E. Saitovitch, K.B. Garg, J. Alloys Compd. 477 (2009) 379–385.
[41] R.O. Ansell, T. Dickinson, A.F. Povey, Corros. Sci. 18 (1978) 245–256.
[42] Y. Umezawa, C.N. Reilley, Anal. Chem. 50 (1978) 1290–1295.
[43] S. Singhal, A.K. Chawla, H.O. Gupta, R. Chandra, Nanoscale Res. Lett. 5 (2010) 323–331.
[44] Ü. Özgür, Y.I. Alivov, C. Liu, A. Teke, M.A. Reshchikov, S. Dogan, V. Avrutin, S.J. Cho, H. Morkoc, J. Appl. Phys. 98 (2005) 041301–041404.
[45] N. Karar, F. Singh, B.R. Mehta, J. Appl. Phys. 95 (2004) 656–661.
[46] R. Sharma, H.S. Bhatti, Nanotechnology 18 (2007) 465703–465710.
[47] R. Kripala, A.K. Gupta, S.K. Mishrab, R.K. Srivastavab, A.C. Pandeyc, S.G. Prakash, Spectrochim. Acta A 76 (2010) 523–530.
[48] G. Murugadoss, B. Rajamannan, V. Ramasamy, J. Lumin. 130 (2010) 2032–2039.
[49] H. Liu, X. Zhang, L. Li, Y.X. Wang, K.H. Gao, Z.Q. Li, R.K. Zheng, S.P. Ringer, B. Zhang, X.X. Zhang, Appl. Phys. Lett. 91 (2007) 072511–072514.
[50] T.T. Quynh Hoa, N. Duc The, S. McVitie, N.H. Nam, L. Van Vu, T.D. Canh, N.N. Long, Opt. Mater. 33 (2011) 308–314.
[51] H.Y. Xu, Y.C. Liu, C.S. Xu, Y.X. Liu, C.L. Shao, R. Mu, J. Chem. Phys. 124 (2006) 074707–074711.
[52] J. Elanchezhiyan, K.P. Bhuvana, N. Gopalakrishnan, T. Balasubramanian, Mater. Lett. 62 (2008) 3379–3381.
[53] W. Chen, L.F. Zhao, Y.Q. Wang, J.H. Miao, S. Liu, Z.C. Xia, S.L. Yuan, Appl. Phys. Lett. 87 (2005) 042507–042510.
[54] H.L. Yan, X.L. Zhong, J.B. Wang, G.J. Huang, S.L. Ding, G.C. Zhou, Y.C. Zhou, Appl. Phys. Lett. 90 (2007) 082503–082506.
[55] C. Bi, L. Pan, M. Xu, L. Qin, J. Yin, in: Proceedings of the Ninth IEEE Conference on Nanotechnology, 2009, pp. 874–877.
[56] S.W. Jung, S.J. An, G.C. Yi, C.U. Jung, S.I. Lee, S. Cho, Appl. Phys. Lett. 80 (2002) 4561–4563.
[57] S. Kolesnik, B. Dabrowski, J. Appl. Phys. 96 (2004) 5379–5381.
[58] S. Delikanli, S. He, Y. Qin, P. Zhang, H. Zeng, H. Zhang, M. Swihart, Appl. Phys. Lett. 93 (2008) 132501–132503.
[59] S. Bhattacharyya, Y. Estrin, D.H. Rich, D. Zitoun, Y. Koltypin, A. Gedanken, J. Phys. Chem. C 114 (2010) 22002–22011.
[60] J. Xie, J. Magn. Magn. Mater. 322 (2010) L37–L41.
[61] D.S. Kim, Y.J. Cho, J. Park, J. Yoon, Y. Jo, M.H. Jung, J. Phys. Chem. C 111 (2007) 10861–10868.
[62] H.T. Xue, P.Q. Zhao, J. Phys. D: Appl. Phys 42 (2009) 015402–015406.
[63] S. Sambasivam, D. PaulJoseph, J.G. Lin, C. Venkateswaran, J. Solid State Chem. 182 (2009) 2598–2601.